Development/Plasticity/Repair

# Modulation of Both Intrinsic and Extrinsic Factors Additively Promotes Rewiring of Corticospinal Circuits after Spinal Cord Injury

Yuka Nakamura,[1,2]* Masaki Ueno,[1,2,3]* Jesse K. Niehaus,[2,3] Richard A. Lang,[4] Yi Zheng,[5] and [ID]Yutaka Yoshida[2,6,7]

[1]Department of System Pathology for Neurological Disorders, Brain Research Institute, Niigata University, Niigata, Niigata 951-8585, Japan, [2]Division of Developmental Biology, Cincinnati Children's Hospital Medical Center, Cincinnati, Ohio 45229, [3]Precursory Research for Embryonic Science and Technology, Japan Science and Technology Agency, Kawaguchi, Saitama 332-0012, Japan, [4]Divisions of Developmental Biology and Ophthalmology, Cincinnati Children's Hospital Medical Center, Cincinnati, Ohio 45229, [5]Division of Experimental Hematology and Cancer Biology, Cincinnati Children's Hospital Medical Center, Cincinnati, Ohio 45229, [6]Neural Connectivity Development in Physiology and Disease Laboratory, Burke Neurological Institute, White Plains, New York 10605, and [7]Feil Family Brain and Mind Research Institute, Weill Cornell Medicine, New York, New York 10065

Axon regeneration after spinal cord injury (SCI) is limited by both a decreased intrinsic ability of neurons to grow axons and the growth-hindering effects of extrinsic inhibitory molecules expressed around the lesion. Deletion of *phosphatase and tensin homolog* (*Pten*) augments mechanistic target of rapamycin (mTOR) signaling and enhances the intrinsic regenerative response of injured corticospinal neurons after SCI. Because of the variety of growth-restrictive extrinsic molecules, it remains unclear how inhibition of conserved inhibitory signaling elements would affect axon regeneration and rewiring after SCI. Moreover, it remains unknown how a combinatorial approach to modulate both extrinsic and intrinsic mechanisms can enhance regeneration and rewiring after SCI. In the present study, we deleted *RhoA* and *RhoC*, which encode small GTPases that mediate growth inhibition signals of a variety of extrinsic molecules, to remove global extrinsic pathways. *RhoA/RhoC* double deletion in mice suppressed retraction or dieback of corticospinal axons after SCI. In contrast, *Pten* deletion increased regrowth of corticospinal axons into the lesion core. Although deletion of both *RhoA* and *Pten* did not promote axon regrowth across the lesion or motor recovery, it additively promoted rewiring of corticospinal circuits connecting the cerebral cortex, spinal cord, and hindlimb muscles. Our genetic findings, therefore, reveal that a combinatorial approach to modulate both intrinsic and extrinsic factors can additively promote neural circuit rewiring after SCI.

*Key words:* corticospinal neuron; motor cortex; Pten; regeneration; RhoA; spinal cord injury

---

## Significance Statement

SCI often causes severe motor deficits because of damage to the corticospinal tract (CST), the major neural pathway for voluntary movements. Regeneration of CST axons is required to reconstruct motor circuits and restore functions; however, a lower intrinsic ability to grow axons and extrinsic inhibitory molecules severely limit axon regeneration in the CNS. Here, we investigated whether suppression of extrinsic inhibitory cues by genetic deletion of *Rho* as well as enhancement of the intrinsic pathway by deletion of *Pten* could enable axon regrowth and rewiring of the CST after SCI. We show that simultaneous elimination of extrinsic and intrinsic signaling pathways can additively promote axon sprouting and rewiring of the corticospinal circuits. Our data demonstrate a potential molecular approach to reconstruct motor pathways after SCI.

---

## Introduction

Spinal cord injury (SCI) causes devastating neurologic deficits in motor, sensory, and autonomic functions. Damages to descending and ascending axons disconnect supraspinal and peripheral regions, leading to chronic impairments. Axon regeneration is required to reconstruct neural circuits and restore functions, but it is severely limited in the adult CNS. The corticospinal tract (CST) is the major neural pathway for voluntary and skilled movements, conveying motor commands from the sensorimotor cortex to the spinal cord (Porter and Lemon, 1993). CST is often damaged by SCI and thus is an important target for regenerative therapies (Oudega and Perez, 2012). Although several approaches have sought to achieve CST regeneration, none have succeeded in full reconstruction of the circuit.

Axon regeneration is limited by both the intrinsic capacity for regeneration as well as extrinsic cues within the injured CNS. Adult neurons lack intrinsic factors for axon growth (Silver et al., 2014; He and Jin, 2016). Studies have demonstrated critical roles for intrinsic signals in axon regeneration (He and Jin, 2016). Several molecules, such as Pten, KLF7, and Sox11, have been discovered to modulate CST regrowth (Liu et al., 2010; Blackmore et al., 2012; Wang et al., 2015). Deletion of *phosphatase and tensin homolog* (*Pten*), a phosphatase that inhibits mechanistic target of rapamycin (mTOR; a critical signaling component for axon growth), drives significant regeneration of CST axons after SCI (Park et al., 2008; Liu et al., 2010), with injured axons robustly extending across the lesion site.

There is a wide variety of extrinsic molecules that have been demonstrated to inhibit axon regrowth. The following three main extrinsic inhibitors are known to prevent regeneration in the lesion: (1) myelin-associated inhibitors (e.g., Nogo, MAG, and OMgp), (2) repulsive axon guidance molecules (e.g., semaphorins, ephrins, Wnts, and RGM), and (3) inhibitory extracellular matrix molecules (e.g., chondroitin sulfate proteoglycan (CSPG; Harel and Strittmatter, 2006; Geoffroy and Zheng, 2014; Silver et al., 2014). Previous studies that abolished or neutralized these molecules have demonstrated increased axon growth; however, the results have been variable, with mixed reports on the success of regeneration after SCI. For example, mice lacking myelin-associated inhibitors and their receptors exhibit regeneration in some studies but not in others (Cafferty et al., 2010; Lee et al., 2010b; Nakamura et al., 2011; Fink et al., 2015). Deletion or inhibition of axon-repulsive molecules also show variable degrees of regeneration (Hata et al., 2006; Lee et al., 2010a; Duffy et al., 2012). We recently showed that *semaphorin* mutant mice suppress dieback of CST axons but do not induce long-distance regeneration over the lesion (Ueno et al., 2020). Suppression or degradation of CSPGs also promote axon regrowth or sprouting, but the amount of regenerating fibers is too low to restore the original circuitry (Bradbury et al., 2002; Wang et al., 2017). These studies suggest that deletion of a singular extrinsic pathway is insufficient to support full regeneration. Importantly, extrinsic molecules are received by specific receptors expressed in injured axons, which converge to a signaling pathway mediated by a small GTPase Rho (McKerracher et al., 2012; Fujita and Yamashita, 2014). RhoA changes actin dynamics and cytoskeletal organization, leading to growth cone collapse and axon growth inhibition. Therefore, Rho may be an ideal target to globally suppress extrinsic signals. Indeed, independent groups have reported that Rho inhibitors enhance axon regeneration (McKerracher et al., 2012; Fujita and Yamashita, 2014). Rho inhibition by C3 transferase (C3) or ibuprofen enhances sprouting and regeneration of corticospinal (CS) axons after SCI (Dergham et al., 2002;

Fu et al., 2007; Boato et al., 2010). Inhibition of the downstream Rho effector Rho-kinase (ROCK) by Y-27632 ROCK inhibitor enhances regeneration after SCI, and *ROCKII* null mutant mice show enhanced regeneration after SCI (Dergham et al., 2002; Fournier et al., 2003; Chan et al., 2005; Duffy et al., 2009). However, the extent of regeneration in these studies is variable. In another study, regenerating fibers were not observed after C3 treatment (Fournier et al., 2003). Because these studies used pharmacological inhibitors, nonspecific targets for molecules and cell types (e.g., neuron vs glial/inflammatory cells) obfuscate the effects of Rho inhibition on axon regrowth. Conditional genetic studies have not been performed to determine the roles of Rho family members in axon regeneration after SCI.

Modulation of both intrinsic and extrinsic pathways is expected to have additive or synergistic effects on axon regeneration and/or rewiring after SCI. For example, a previous study used the combinatorial approach of deleting both *Pten* and *Nogo* and showed an additive effect on axon regeneration (Geoffroy et al., 2015). As there are a variety of extrinsic pathways in the injured spinal cord, the combinatory effects of *Pten* deletion and a global inhibition of extrinsic signals (e.g., *RhoA* deletion) needs to be determined. In the present study, we examined whether codeletion of *RhoA* and *Pten* facilitates regeneration and/or sprouting of CST axons to reconstruct CS circuits disrupted by SCI. Our results demonstrate that deletion of both *RhoA* and *Pten* additively enhance CS axon rewiring after SCI.

## Materials and Methods

*Animals.* C57BL/6J mice (The Jackson laboratory), *RhoA^f/f* (Chauhan et al., 2011; Katayama et al., 2011; Melendez et al., 2011), *RhoC^−/−* (a gift from Tak W. Mak, University Health Network (Hakem et al., 2005)), *Pten^f/f* (The Jackson laboratory; Lesche et al., 2002), and *CAG-lox-CAT-lox-EGFP* mice (Nakamura et al., 2006) were used. *RhoA^f/f*, *RhoC^−/−*, and *Pten^f/f* mice were backcrossed with C57BL/6 mice for at least seven generations. All mice were maintained on a C57BL/6 background. Procedures were performed in accordance with protocols approved by the Institutional Animal Care and Use Committee of the Cincinnati Children's Hospital Medical Center and Niigata University.

*Neurite outgrowth assay.* The neurite outgrowth assay was performed as previously described with some modifications (Nakamura et al., 2011). Cerebellar granule neurons (CGNs) of P7 mice (*RhoA^f/f*, *RhoA^f/f;RhoC^−/−*, and *Pten^f/f* mice) were cultured in serum-free DMEM/F12 medium supplemented with 2% B-27 supplement and penicillin/streptomycin (Invitrogen) in six-well culture plates ($2 \times 10^6$ cells/well). Adeno-associated virus (AAV) expressing a fusion protein EGFP-Cre, tagged with a nuclear localization sequence under the human synapsin-1 promoter [3 μl; AAV1-Syn-EGFP-Cre (AAV-Cre), $4.3 \times 10^{12}$ GC/ml; Penn Vector Core] was added to each well. After 6 d, cells were trypsinized and replated on four-well chamber slides ($5 \times 10^4$ cells/well) precoated with 100 μg/ml poly-L-lysine (Sigma-Aldrich) and Nogo-A-Fc (3 μl spot, 100 ng/μl; catalog #3728-NG; R&D Systems) or CSPG (5 μl spot, 200 ng/ml; catalog #CC117, Millipore) overnight and then with laminin (10 μg/ml, Invitrogen) for 2 h before plating. CGNs were cultured for 48 h in serum-free DMEM/F12 medium supplemented with 2% B-27 supplement and penicillin/streptomycin. Cells were then fixed with 4% paraformaldehyde (PFA) for 30 min and immunostained with a chick anti-βIII-tubulin antibody (Tuj1, 1:200; catalog #AB9345, Millipore) and Alexa Fluor 568 donkey anti-chick IgY antibody (1:500; Invitrogen). Fields of neurons were selected randomly and photographed using a fluorescence microscope (Zeiss Axio Imager Z1). Neurite lengths were measured using ImageJ software (National Institutes of Health).

*Spinal cord injury.* Adult female mice (8 weeks of age) were subjected to SCI as previously reported (Nakamura et al., 2011; Ueno et al., 2020). Mice were anesthetized with isoflurane. A laminectomy was performed to expose the spinal cord, and a dorsal hemisection (depth of 1.0 mm)

was performed at T9–10 with a number 11 surgical blade to completely sever the dorsal and dorsolateral CSTs. The muscle layers and skin on the back were then sutured, and the mice were placed in cages in a pathogen-free environment under a 12 h light/dark cycle and fed commercial pellets and water *ad libitum*. Bladders were manually expressed daily.

*AAV injection and anterograde tracing.* Injections were performed as previously reported (Ueno et al., 2012, 2020). Mice were anesthetized and placed in a stereotaxic frame. The scalp was incised, and small holes were made at the corresponding sites of injections of the skull by using a 27 gauge needle. To examine the regeneration of CST fibers, AAV-Cre [$4.3 \times 10^{12}$ GC/ml; Penn Vector Core] was injected into the right and left hindlimb sensorimotor cortices (depth of 0.5 mm; coordinates, 0.8 mm posterior, 1.2 mm lateral to the bregma, 0.6 µl per cortex) using a Hamilton syringe tipped with a glass micropipette, 2 weeks before the injury. Biotinylated dextran amine [BDA; molecular weight, 10,000; 10% in PBS; Invitrogen], an anterograde tracer, was then injected at each of the four sites in the right and left hemispheres (depth of 0.5 mm; coordinates, 0.6–1.2 mm posterior, 0.8–1.4 mm lateral to the bregma, and 0.4 µl/site) at day 42 postinjury. The mice were perfused 2 weeks later for histologic analyses.

To examine CST axon dieback at day 10 postinjury, AAV1-Syn-EGFP-Cre ($2.15 \times 10^{12}$ GC/ml) and AAV1-CAG-FLEX-tdTomato ($1.97 \times 10^{12}$ GC/ml; Penn Vector Core) were injected into the left and right hindlimb sensorimotor cortices (depth of 0.5 mm; coordinates, 0.6 mm posterior, 1.2 mm lateral to the bregma, and 0.2 µl/site) 2 weeks before the injury. The mice were perfused 10 d after SCI for histologic analyses. We used the double AAV injections instead of BDA because our pilot study indicated that BDA injection 10 d after AAV-Cre injection significantly decreased labeling efficiency.

To examine the sprouting of CST fibers, AAV1-Syn-EGFP-Cre ($2.15 \times 10^{12}$ GC/ml) and AAV1-CAG-FLEX-tdTomato ($1.97 \times 10^{12}$ GC/ml) were injected in the left hindlimb sensorimotor cortex (depth of 0.5 mm; coordinates, 0.6 mm posterior, 1.2 mm lateral to the bregma, and 0.2 µl/site), and AAV1-Syn-EGFP-Cre ($2.15 \times 10^{12}$ GC/ml) was injected into the right side, 2 weeks before the injury. The mice were perfused 56 d after SCI for histologic analyses.

*Pseudorabies virus (PRV) trans-synaptic tracing.* GFP- or RFP-expressing PRV (PRV152, expressing GFP, $4.9 \times 10^{9}$ pfu/ml; PRV614, expressing RFP, $3.9 \times 10^{9}$ pfu/ml; gifts from Lynn Enquist, Princeton University) was injected (5 µl) into the rectus femoris (Rf) or biceps femoris (Bf) muscle of the right hindlimb by using a glass capillary. Under anesthesia with isoflurane, a skin incision was made to expose the target muscle. PRV was injected into the muscle using a glass capillary (total 5 µl), and the skin was sutured. Animals were kept for 6 d and then killed for histologic analyses. In pilot studies, we determined that day 5 was the time point at which PRVs trans-synaptically infected and expressed fluorescent proteins in third-order neurons of the sensorimotor cortex in control mice, but 6 d were required to observe PRV-labeled cells in SCI mice (Ueno et al., 2020), which may be because of limited viral uptake in SCI mice or viral spread through other, less direct connections to fourth-order cerebral neurons.

*Immunohistochemistry.* The animals were perfused transcardially with 4% PFA in phosphate buffer at the indicated time points after the SCI. The brain and spinal cord were dissected and postfixed in the same fixatives overnight. The tissues were then cryopreserved in 30% sucrose in PBS overnight and embedded in Tissue-Tek optimal cutting temperature compound (Sakura Finetek). Serial 20- or 50-µm-thick sections were made with a cryostat and mounted on SuperFrost Plus slides (Fisher Scientific) or MAS-coated slides (Matsunami). For immunohistochemistry, the sections were blocked with 1% bovine serum albumin (BSA) in 0.3% Triton X-100/PBS for 2 h and then incubated with the following primary antibodies overnight at 4°C: mouse anti-GFAP (1:400; catalog #G3898, Sigma-Aldrich), rabbit anti-GFP (1:1000; catalog #A11122, Invitrogen), sheep anti-GFP (1:1000; catalog #4745-1051, Serotec), rabbit anti-Pten (1:100; catalog #9188, Cell Signaling Technology), rabbit anti-phospho-S6 ribosomal protein (1:400; catalog #4858, Cell Signaling Technology), rabbit anti-RFP antibody (1:1000; catalog #600-401-379, Rockland), goat anti-mCherry (1:1000; catalog #AB0040-200,

Sicgen), guinea pig anti-Vglut1 (1:10,000; catalog #AB5905, Millipore), or rabbit anti-PSD-95 (1:200; catalog #516900, Invitrogen). After washing with 0.1% Tween 20/PBS, the sections were incubated with the following secondary antibodies for 2 h at room temperature: Alexa Fluor 488 or 568 donkey anti-rabbit, mouse, sheep, or goat IgG antibody (1:500; Invitrogen) or Alexa Fluor 647 donkey anti-guinea pig IgG antibody (1:1000; Jackson ImmunoResearch). The sections were then washed with PBS and counterstained with DAPI (1 µg/ml; Santa Cruz Biotechnology) to visualize nuclei.

For BDA labeling, the sections were incubated with 0.3% Triton X-100/PBS for 4 h and then with Alexa Fluor 568 conjugated streptavidin (1:400; Invitrogen) for 2 h at room temperature. Images were acquired using a fluorescence microscope (Zeiss Axio Imager Z1 or Olympus BX51, DP71) or confocal microscopy (Olympus FV3000).

*In situ hybridization.* The cDNA fragments encoding *RhoA* (NM_016802.5; 550–1051) and *RhoC* (NM_007484.2; 117–649) were obtained by PCR from cDNA collected from the cerebral cortex at P1. Digoxigenin-labeled riboprobes were prepared by *in vitro* transcription from the amplified products. *In situ* hybridization was performed as described previously (Ueno et al., 2020). Signals were detected using alkaline phosphatase-coupled anti-digoxigenin antibodies (Roche Diagnostics) with nitroblue tetrazolium and 5-bromo-4-chloro-3-indolyl phosphate as substrates for the color reaction. The sections were further processed for immunohistochemistry with an anti-GFP antibody.

*Quantification of CST dieback, axonal regrowth, and sprouting.* To quantify the dieback and regeneration of CST axons, BDA-labeled pixel areas of CST fibers in the dorsal column were measured at each 100 µm distance bin from the lesion border by ImageJ software (Ueno et al., 2020). The lesion border was defined as the border between the GFAP-positive and negative areas, which correspond to the astroglial and fibrotic scars, respectively (Liu et al., 2008; Herrmann et al., 2010). Four to seven sections that included BDA$^+$ dorsal CST axons were assessed per animal. To normalize interanimal differences in tracing volumes, the BDA$^+$ area at each distance was divided by the average BDA$^+$ area in the rostral 600–700 and 700–800 µm bins, and the value was defined as the axon index.

To assess CST axon regrowth into the lesion, BDA-positive pixel areas of CST fibers caudal to the border of the glial and fibrotic scars were measured in every second serial sagittal section (20 µm), and the total area was normalized by the BDA$^+$ area of the dorsal CST in the rostral 600–800 µm bin as described above.

To assess CST sprouting, tdTomato-positive pixel areas of CST fibers in the gray matter were measured in every fifth serial transverse section (20 µm), and the total area in 0–300, 400–600, and 700–1000 µm rostral regions were calculated and normalized by the average number of tdTomato$^+$ fibers in the dorsal CST in sections 900 and 1000 µm rostral to the lesion.

*Quantification of PRV$^+$ neurons.* Serial 50-*µ*m-thick coronal cortical sections were made, and images of every other section were acquired by fluorescence microscopy. The positions of PRV-GFP- and RFP-labeled cells along the mediolateral (ML) and anteroposterior (AP) axes (ML, 0 mm at midline; AP, 0 mm at the bregma; Paxinos and Franklin, 2001) were plotted using ImageJ software (Point Picker, National Institutes of Health), and the total number of PRV$^+$ cells was counted. In the experiments using AAV-Cre, PRV-RFP and EGFP-Cre double-positive cells were plotted and counted.

*Western blot.* Dissected brains of wild-type (WT) or *RhoA$^{f/f}$* mice injected with AAV-Cre were sectioned by using a vibratome (300 µm thick, Leica), and the sensorimotor areas, including layer V, were collected. CGNs cultured from P7 *RhoA$^{f/f}$* mice with and without AAV-Cre infection were collected at day 6 *in vitro*. They were then homogenized in lysis buffer (50 mM Tris-HCl, pH 8.0, containing 150 mM NaCl, 0.1% SDS, 0.5% sodium deoxycholate, 1% NP-40, and protease inhibitor cocktail; Roche). After centrifugation at $12,000 \times g$ for 20 min at 4°C, proteins were separated on SDS-PAGE and transferred to a PVDF membrane (Millipore Sigma). The membrane was blocked with 5% nonfat dry milk in PBS containing 0.05% Tween 20 and then incubated with rabbit anti-RhoA (1:1000; catalog #2117, Cell Signaling Technology),

rabbit anti-RhoC (1:1000; catalog #3430, Cell Signaling Technology), or mouse TuJ1 (1:1000; catalog #MMS-435P, Covance) overnight at 4°C. After washing, the membrane was incubated with HRP-linked anti-mouse IgG or anti-rabbit IgG antibody (1:5000; Santa Cruz Biotechnology). The detection was performed with a Luminata Forte Western HRP Substrate (Millipore).

*Behavioral analyses.* Motor behavior tests were performed as previously reported (Nakamura et al., 2011; Ueno et al., 2020). Hindlimb locomotor performance of stepping and coordination in movement was analyzed by using the Basso Mouse Scale (BMS) open-field score (Basso et al., 2006). Motor performance was scored with 9-point scale and 11-point scales for subscore at days 3, 7, 14, 21, 28, 35, and 42 after SCI.

The grid walk test assesses the ability of an animal to accurately place its hindpaws on the rungs of a grid during spontaneous exploration. Mice were trained to walk on a wire grid (0.35 m long with 10 mm squares) before the surgery. The number of foot slips in which the hind paw dropped below the grid plane was counted during 50 steps of exploration on days 7, 14, 21, 28, 35, and 42 after SCI, and the percentage of foot slips was calculated.

*Experimental design and statistical analyses.* For the numbers of experiments or animals used in each experiment see below, Results, and figure legends. We based our sample sizes on a previous study in our laboratory that used similar histologic methods (Ueno et al., 2020). Neurite outgrowth assays were performed for each genotype and substrate condition in 4–5 independent experiments (Fig. 1). For the BDA-injection experiments (see Fig. 3), 5–6 animals of each genotype were injected with AAV-Cre at 6 weeks of age, subjected to SCI 2 weeks later, and injected with BDA at day 42 postinjury. These animals were perfused at day 56. For PRV experiments (see Fig. 5), four animals of each genotype were injected with AAV-Cre at 6 weeks of age, received SCI 2 weeks later, were injected with PRV at day 42 postinjury, and were perfused 6 d later. For the sprouting fiber analyses (see Fig. 6), four animals of each genotype were injected with AAV-Cre and AAV-CAG-FLEX-tdTomato at 6 weeks of age, received SCI 2 weeks later, and were perfused at day 56 postinjury. For behavioral analyses (see Fig. 6), the motor performance of 12 to 14 animals of each genotype were tested weekly preinjury and postinjury. Quantitative data are represented as the mean ± SEM. Statistical analyses were performed using Prism 6 (GraphPad). Differences among groups were statistically analyzed by one-way ANOVA followed by Tukey's test or two-way repeated-measures ANOVA followed by Bonferroni's test. A $p$ value of <0.05 was considered statistically significant.

# Results

## Genetic deletion of *Rho* and *Pten* attenuates axonal growth inhibition by extrinsic inhibitory molecules *in vitro*

Previous studies have indicated that Rho is activated in response to inhibitory molecules and that inhibition of Rho or the down-stream signaling molecule ROCK decreases axon growth inhibition (Dergham et al., 2002; Borisoff et al., 2003; Fournier et al., 2003; Monnier et al., 2003; Duffy et al., 2009). However, it remains unknown whether genetic *RhoA* deletion suppresses growth inhibition. We first tested whether *RhoA* deletion affects axon growth inhibition by Nogo and CSPG *in vitro*. We used CGNs that are widely used to assess neurite outgrowth on inhibitory substrates, including Nogo and CSPG *in vitro* (Atwal et al., 2008; Usher et al., 2010). CGNs were collected from pups of *RhoA*-floxed (*RhoA^f/f^*) mice, and transduced with AAV-expressing EGFP-Cre under the human synapsin 1 promoter (AAV-Cre in this study) to recombine and delete *RhoA*. *RhoA*-deficient neurons were then replated onto Nogo- or CSPG-coated culture dishes, and neurite lengths were measured 2 d later. Nogo and CSPG significantly reduced neurite outgrowth in control CGNs. *RhoA* deletion rescued the inhibitory effects of Nogo (Fig. 1A,B; $n = 5$; $p = 0.0127$) and showed a trend toward increased neurite length on the CSPG substrate, although this was not statistically

significant (Fig. 1A,C; $n = 4$; $p = 0.183$). As *RhoA* deletion has previously been shown to increase the expression of its homolog, RhoC (Melendez et al., 2011; Leslie et al., 2012; Mulherkar et al., 2013), CGNs collected from *RhoA^f/f^*;*RhoC^−/−^* mice were further tested in the neurite outgrowth assay. Similar to *RhoA* single knockout, *RhoA* and *RhoC* double knockout rescued the outgrowth inhibition by Nogo, which had a larger effect than the *RhoA* single knockout (Fig. 1A,D; $n = 4$–5; $p = 0.0117$). The double knockout also showed a nonsignificant trend toward attenuating the growth inhibition of CSPG (Fig. 1A,E; $n = 4$; $p = 0.156$). These results indicated that genetic deletion of *RhoA* and *RhoC* can partially overcome the effects of axon growth inhibitors.

We next examined the effect of *Pten* deletion on inhibitory molecules. CGNs obtained from postnatal *Pten^f/f^* mice were similarly treated with AAV-Cre and replated on Nogo or CSPG-coated dishes. *Pten*-deletion in neurons rescued the inhibitory effects of Nogo and CSPG, resulting in neurite lengths that were similar to those on the control substrate (Fig. 1A,F,G; $n = 4$; $p = 0.0024$, *Pten^f/f^* vs *Pten^f/f^* + AAV-Cre on Nogo; $p = 0.0015$, *Pten^f/f^* vs *Pten^f/f^* + AAV-Cre on CSPG). These results demonstrated the strong potency of intrinsic *Pten* deletion in driving axon growth. Together, these data indicated that genetic deletion of either *Rho* or *Pten* promotes neurite growth in an inhibitory environment.

## Genetic deletions of *RhoA* and *RhoC* suppress axon dieback after SCI

We next investigated whether *Rho* and *Pten* deletions in mice affect CST axonal length after SCI. To delete *RhoA* or *Pten* in CS neurons, we injected AAV-Cre into the hindlimb area of the sensorimotor cortex of *RhoA^f/f^* or *Pten^f/f^* mice. For SCI, a dorsal hemisection was performed at the thoracic level 9–10 to completely transect the dorsal and dorsolateral CST (Steward et al., 2008).

First, to test the recombination efficiency of *RhoA*, AAV-Cre was injected into the cerebral cortex of *RhoA^f/f^* mice crossed with *lox-CAT-lox-EGFP* (*lcl-EGFP*) reporter mice (Nakamura et al., 2006). After SCI, recombined EGFP signals were clearly detected in the cortex and transected CST fibers, suggesting that Cre efficiently induced recombination in CS neurons (Fig. 2A,B). The axonal EGFP signals originating from the reporter mice were discriminated from AAV-derived fusion EGFP-Cre signals in the nuclei by the tagged nuclear localization sequence. Next, RhoA expression was examined 2 weeks after AAV-Cre injection in *RhoA^f/f^* mice. Nuclear EGFP-Cre signals were clearly detected in the cortex, including in layer V (Fig. 2C). At the injection site, *in situ* hybridization and Western blot analyses showed that *RhoA* mRNA and protein expression were decreased, respectively (Fig. 2C,D). We further examined RhoC expression, which has been reported to be increased after *RhoA* deletion (Melendez et al., 2011; Leslie et al., 2012; Mulherkar et al., 2013). Although *RhoC* mRNA in the contralateral side of the AAV-injected cerebral cortex of *RhoA^f/f^* mice was below the detection limit by *in situ* hybridization, the signal appeared to be increased in the injection site of those mice (Fig. 2C). The RhoC protein level was also elevated (Fig. 2D). Next, *Pten* deletion was examined in the cortex of *Pten^f/f^* mice. As previously reported (Liu et al., 2010), AAV-Cre injection reduced Pten expression and increased phosphorylated S6 ribosomal protein, an indicator of the mTOR pathway (Fig. 2E). These findings suggest that *Pten* deletion enhances translational activity via the mTOR pathway in the cerebral cortex.

The animals were subjected to dorsal hemisection SCI 2 weeks after AAV-Cre injection, and BDA, an anterograde
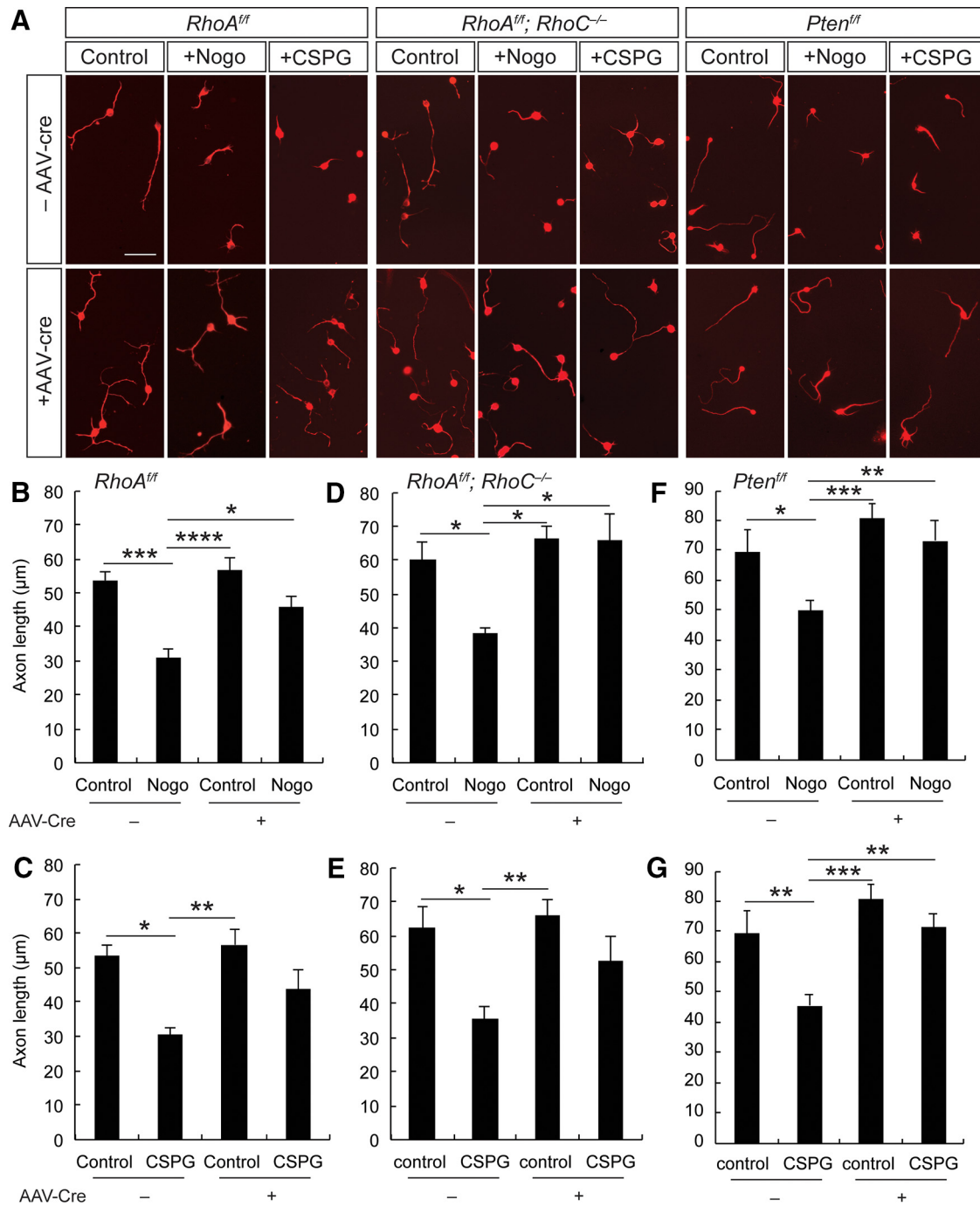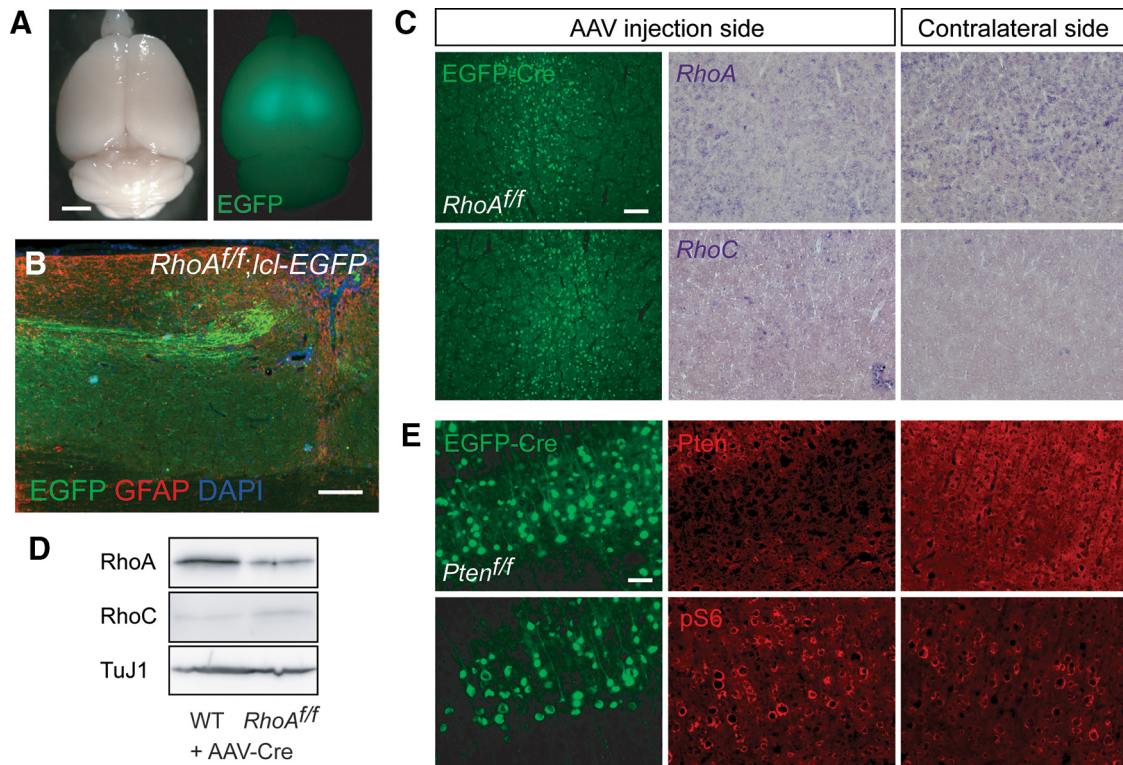
**Figure 1.** Genetic deletion of *RhoA* and *Pten* promotes axon growth on inhibitory substances *in vitro*. **A**, Representative images of neurite outgrowth of CGNs of *RhoA^{f/f}*, *RhoA^{f/f};RhoC^{−/−}*, and *Pten^{f/f}* mice treated with and without AAV-Cre on control, Nogo, and CSPG substrates. Scale bar, 50 μm. **B–G**, Quantitative data of neurite lengths of CGNs of *RhoA^{f/f}* (**B**, **C**), *RhoA^{f/f}; RhoC^{−/−}* (**D**, **E**), and *Pten^{f/f}* (**F**, **G**) mice treated with and without AAV-Cre treatment on control, Nogo (**B**, **D**, **F**), and CSPG substrates (**C**, **E**, **G**). One-way ANOVA and Tukey's test, *$p < 0.05$, ** $p < 0.01$, ***$p < 0.001$, ****$p < 0.0001$, $n = 4$–5.

tracer, was then injected into the hindlimb region of the sensori-motor cortex to label the CST at day 42. CST regeneration was analyzed histologically at day 56 after SCI. In WT mice, the transected CST axons were observed mainly $500 \, \mu m$ from the rostral to the lesion in the dorsal funiculus, indicating that injured CST axons had retracted, which is called axon dieback (Fig. 3A; Ueno et al., 2020). In contrast, 80% of injured CST axons in *RhoA^{f/f}* mice tended to remain within $300 \, \mu m$ from the lesion border between the GFAP⁺ glial scar and GFAP⁻ fibrotic scar (Herrmann et al., 2010), although the distance was not

statistically significant compared with that of WT mice (Fig. 3B,G; WT, $n = 5$; *RhoA^{f/f}*, $n = 6$; $p = 0.312$). Because *RhoA* deletion increased levels of *RhoC* expression (Fig. 2C,D), we next generated *RhoA^{f/f};RhoC^{−/−}* mice and transduced them with AAV-Cre. In these animals, most CST axon endings were located within $400 \, \mu m$ from the lesion site (Fig. 3C,G; $n = 5$; $p = 0.0036$). To discriminate between reduced axon dieback and regeneration, we labeled CST axons before SCI and then quantified them at 10 d post-SCI, when axon dieback typically begins (Liu et al., 2010). Similar to our findings at day 56, we found that CST axons

**Figure 2.** Genetic deletion of *RhoA* and *Pten* in the sensorimotor cortex. ***A***, Representative brain images injected with AAV-Cre (AAV1-Syn-EGFP-Cre) into the hindlimb area of the sensorimotor cortex of *RhoA*$^{f/f}$;*lcl-EGFP* mice. Right, Bilateral EGFP expression in the cerebral cortex. Scale bar, 2 mm. ***B***, GFP-labeled CST fibers (green) in the thoracic SCI lesion of *RhoA*$^{f/f}$;*lcl-EGFP* mice with AAV-Cre injection at day 28 postinjury. Sagittal section stained with GFP (green), GFAP (red), and DAPI (blue); left, rostral. Scale bar, 200 μm. ***C***, Representative images of *RhoA* and *RhoC* mRNA expression in the AAV-Cre-injected site of the sensorimotor cortex of *RhoA*$^{f/f}$ mice at 2 weeks postinjection as detected by *in situ* hybridization (middle). Right, The mRNA expression in the contralateral side of the cortex. Left, EGFP-Cre (green) expression detected by immunohistochemistry; coronal sections. Scale bar, 100 μm. ***D***, Expression of RhoA and RhoC proteins in the injection site of the cerebral cortex in WT and *RhoA*$^{f/f}$ mice with AAV-Cre injection at 2 weeks postinjection as detected by Western blotting. ***E***, Pten and phosphorylated S6 ribosomal protein (pS6) expression in the sensorimotor cortex of *Pten*$^{f/f}$ mice injected with AAV-Cre at 2 weeks postinjection as detected by immunohistochemistry (middle). Right, Expression in the contralateral side of the cortex. Left, EGFP-Cre expression (green). Scale bar, 50 μm.

in *RhoA*$^{f/f}$;*RhoC*$^{-/-}$ mice remained within 400 μm from the lesion site at day 10, indicating that significantly less dieback was detected in *RhoA*$^{f/f}$;*RhoC*$^{-/-}$ mice compared with that observed in control mice (Fig. 3H,I; n = 5; p = 0.0458). Although there was less dieback from *RhoA*- or *RhoA/RhoC*-deleted axons, these axons did not regenerate beyond the border of the glial and fibrotic scar or extend caudal to the lesion (Fig. 3B,C,K). These results suggest that Rho inhibition suppresses axon retraction or dieback but has limited effects on axon regeneration beyond the lesion.

**Genetic deletion of *Pten* with *RhoA* and *RhoC* suppresses axon dieback and promotes regeneration after SCI**
To examine the effects on regeneration by targeting both extrinsic and intrinsic factors, *Pten*-deleted mice were further evaluated. First, *Pten*$^{f/f}$ mice were injected with AAV-Cre, and CST regeneration was examined. At day 56 postinjury, 80% of the main CST axons were found within 300 μm from the lesion border, similar to observations following *RhoA* deletion (Fig. 3D,G; n = 5; p = 0.1628). In contrast to WT and *Rho* mutant mice, however, several individual CST axons were observed to have regenerated beyond the glial-fibrotic border (Fig. 3J,K). The pattern of regenerating axons was partially consistent with previous reports of *Pten* deletion in adult mice (Liu et al., 2010; Du et al., 2015), although the axons in our study did not elongate across the lesion.

We next examined the regenerative responses of CST axons in *RhoA*$^{f/f}$;*Pten*$^{f/f}$ double-floxed mice with AAV-Cre injection. In

this mouse line, we observed similar axon dynamics to those of *Pten*$^{f/f}$ mice. The majority of CST axon endings in the dorsal funiculus were found within 300 μm of the rostral lesion boundary, but this increase was not significant compared with WT mice (Fig. 3E,G; n = 6; p = 0.2985). As in single *Pten*-deleted mice, we observed axons growing into the lesion core, but they did not extend caudal to the lesion (Fig. 3J,K). Finally, we examined the injured CST fibers in *RhoA*$^{f/f}$;*RhoC*$^{-/-}$;*Pten*$^{f/f}$ mice with AAV-Cre injection. In this condition, axon behaviors appeared similar to what was observed in *RhoA*$^{f/f}$;*RhoC*$^{-/-}$ and *Pten*$^{f/f}$ mice. Most CST axon endings in the dorsal funiculus were located within 400 μm of the rostral lesion boundary, similar to the observations in *RhoA*$^{f/f}$;*RhoC*$^{-/-}$ mice (Fig. 3F,G; n = 5; p = 0.0158). In addition, axons grew into the lesion core similar to that observed in *Pten*$^{f/f}$ and *RhoA*$^{f/f}$;*Pten*$^{f/f}$ mice (Fig. 3J,K).

Collectively, these results indicate the following: (1) *RhoA/RhoC* deletion attenuates axon dieback, (2) *Pten* deletion induces axon regeneration into the lesion, and (3) combinational targeting of *Rho* and *Pten* has additive effects to suppress dieback and induce regeneration in injured CST axons. Despite this effect, the combinational approach did not induce regenerating axons to elongate through the fibrotic core of the scar and extend caudal to the lesion.

**Genetic deletions of *Pten* and *RhoA* promote rewiring of CS circuits after SCI**
As regenerating CST axons did not project across the lesion after *Rho* and *Pten* deletion, we next tested whether *Rho* and *Pten*
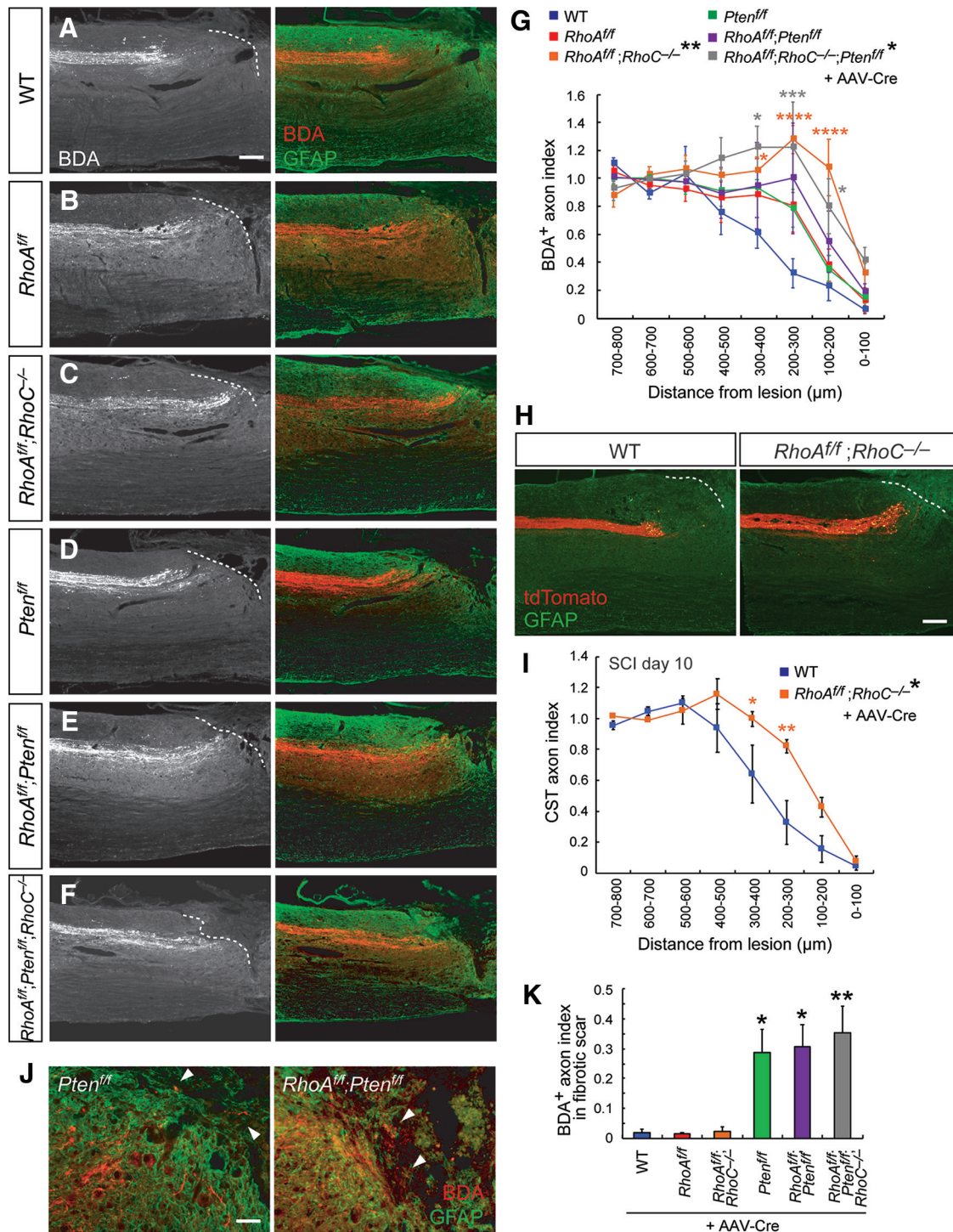
**Figure 3.** *RhoA/RhoC* deletion suppresses axon dieback, and *Pten* deletion induces axon regeneration of the CST after SCI. *A–F*, Representative images of BDA-labeled CST axons in the thoracic cord rostral to the lesion in WT (*A*), *RhoA^f/f* (*B*), *RhoA^f/f;RhoC^−/−* (*C*), *Pten^f/f* (*D*), *RhoA^f/f;Pten^f/f* (*E*), and *RhoA^f/f;Pten^f/f;RhoC^−/−* (*F*) mice injected with AAV-Cre. Sagittal view of the thoracic cord at day 56 postinjury. Dotted lines indicate the border of the GFAP^+ glial scar and the GFAP^− fibrotic scar. Left, BDA (white); right, BDA (red) and GFAP (green) staining. Scale bar, 200 μm. *G*, Quantification of CST axon amounts in the dorsal funiculus rostral to the lesion in WT (*n* = 5), *RhoA^f/f* (*n* = 6), *RhoA^f/f;RhoC^−/−* (*n* = 5), *Pten^f/f* (*n* = 5), *RhoA^f/f;Pten^f/f* (*n* = 6), and *RhoA^f/f;Pten^f/f;RhoC^−/−* mice (*n* = 5). Two-way repeated-measures ANOVA followed by Bonferroni's test, *p < 0.05, **p < 0.01, ***p < 0.001, ****p < 0.0001. *H*, Representative images of tdTomato-labeled CST axons in the thoracic cord rostral to the lesion at day 10 postinjury in WT (left) and *RhoA^f/f;RhoC^−/−* mice (right) injected with AAV-Cre and AAV-CAG-FLEX-tdTomato; tdTomato (red) and GFAP (green) staining. Scale bar, 200 μm. *I*, Quantification of CST axon amounts in the dorsal funiculus rostral to the lesion in WT (*n* = 5) and *RhoA^f/f;RhoC^−/−* mice (*n* = 5). Two-way repeated-measures ANOVA followed by Bonferroni's test, *p < 0.05, **p < 0.01. *J*, Representative images of BDA^+ CST fibers growing beyond the border of the glial and fibrotic scar (arrowheads) in *Pten^f/f* (left) and *RhoA^f/f;Pten^f/f* mice (right). Scale bar, 50 μm. *K*, Quantification of CST fibers growing beyond the border of the glial and fibrotic scars in WT (*n* = 5), *RhoA^f/f* (*n* = 6), *RhoA^f/f;RhoC^−/−* (*n* = 5), *Pten^f/f* (*n* = 5), *RhoA^f/f;Pten^f/f* (*n* = 6), and *RhoA^f/f;Pten^f/f;RhoC^−/−* mice (*n* = 5). One-way ANOVA followed by Tukey's test, *p < 0.05, **p < 0.01.
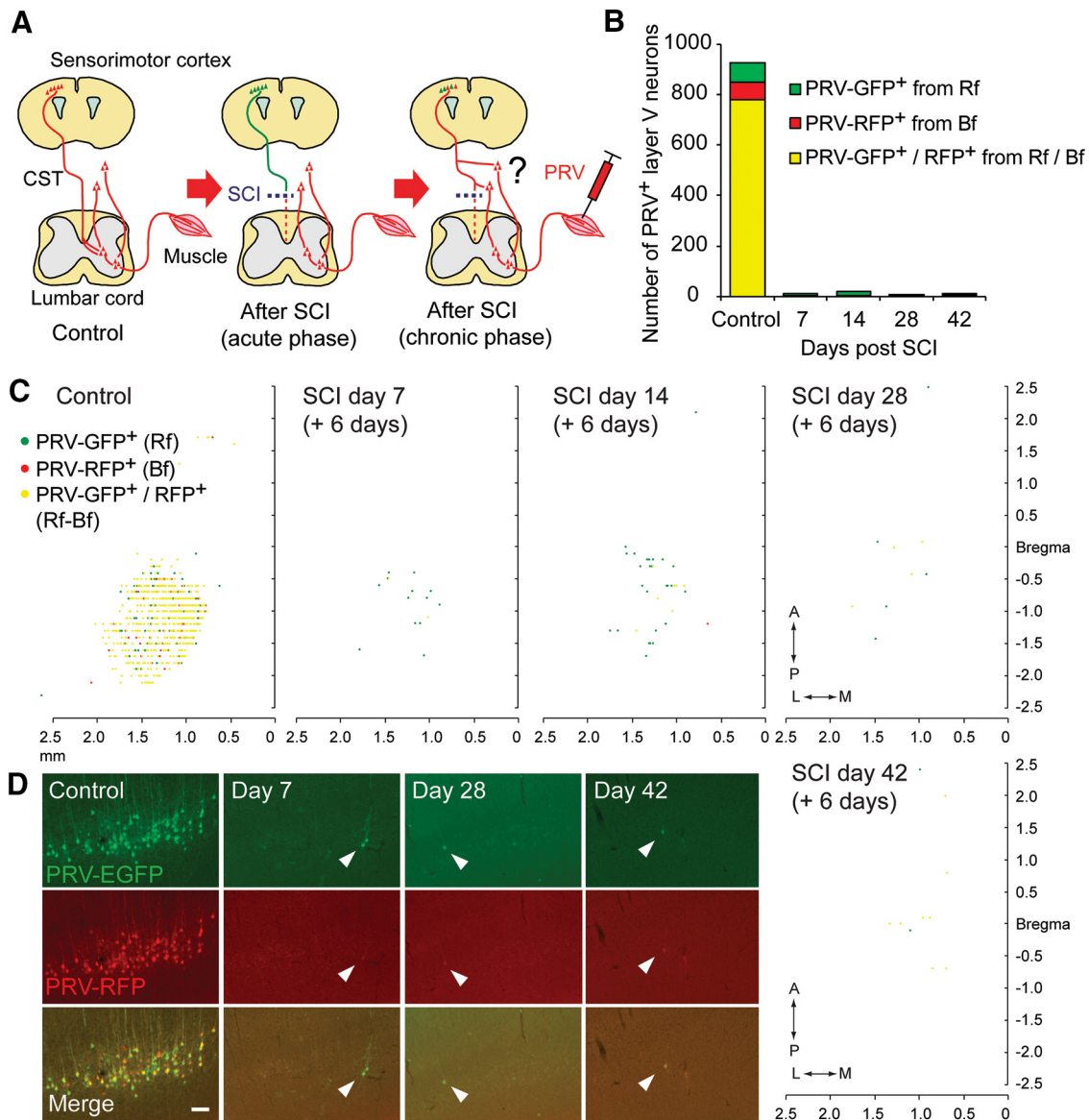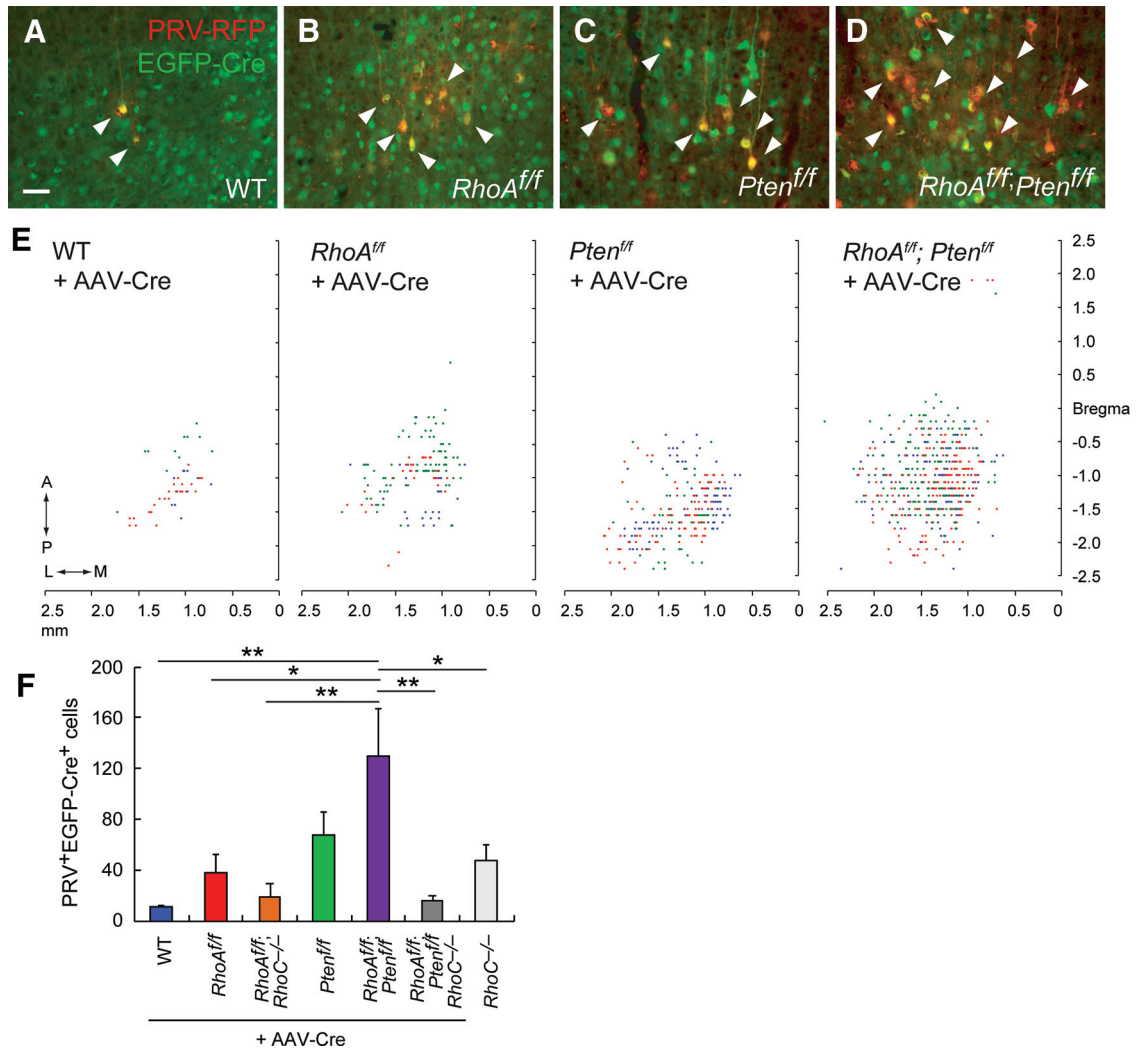
**Figure 4.** Sensorimotor cortex to spinal cord to hindlimb connections are not increased during the post-SCI recovery period in WT mice. **A**, Schematic illustration to label rewired CS circuits by trans-synaptic tracing with PRV injected into hindlimb muscles. **B**, The numbers of PRV$^+$ neurons were counted in the sensorimotor cortex 6 d after PRV injection in control and SCI mice at days 7, 14, 28, and 42 postinjury; $n = 2$. The average number of PRV-GFP$^+$ neurons traced from the Rf muscle is shown in green. PRV-RFP$^+$ neurons traced from the Bf muscle are shown in red. PRV-GFP/PRV-RFP double-positive neurons are shown in yellow. **C**, Top views of the cortical locations of PRV$^+$ layer V neurons in the cerebral cortices of representative control and SCI mice injected at days 7, 14, 28, and 42 d postinjury. PRV$^+$ cells were plotted by the distance from the bregma along the AP and ML axes in top views of the cortex. PRV-GFP$^+$ neurons traced from the Rf muscle are shown in green. PRV-RFP$^+$ neurons traced from the Bf muscle are shown in red. PRV-GFP$^+$/PRV-RFP$^+$ neurons traced from Rf/Bf are shown in yellow. **D**, Representative images of PRV-GFP$^+$ and RFP$^+$ layer V neurons in the sensorimotor cortex of control and SCI mice on days 7, 14, and 42 postinjury. Scale bar, 100 μm.

deletion enhances rewiring of the CS circuits postinjury. Injured axons exhibit two different modes of growth, (1) regeneration, in which axons regrow from the tips of transection, and (2) sprouting, in which axons generate collaterals from the middle of the axon shaft, or defined as regenerative sprouting that generates collaterals from injured axons (Tuszynski and Steward, 2012; Geoffroy and Zheng, 2014). In particular, regenerative sprouting CST collaterals can rewire to target surviving propriospinal neurons in the rostral area of the lesion, thus creating detour circuits that connect with lumbar motor neurons to control hindlimb muscle movements (Fig. 4A; Bareyre et al., 2004).

To investigate whether CST rewiring is enhanced by *Rho* or/ and *Pten* deletion, we used RFP (or GFP)-expressing PRV (PRV614 and PRV152, respectively), a trans-synaptic and

retrograde viral tracer, to label neurons in the circuitry connecting sensorimotor cortex to spinal cord to hindlimb muscle (Fig. 4A; Gu et al., 2017). First, we injected PRV152 into the hindlimb Rf muscle and PRV614 into the hindlimb Bf muscle at days 7, 14, 28, and 42 after SCI in WT mice and observed PRV-GFP$^+$ and PRV-RFP$^+$ layer V neurons postinjection. In intact mice, a number of PRV$^+$ neurons were located in the hindlimb area of the sensorimotor cortex just caudal to the bregma (Fig. 4; Tennant et al., 2011). The number of PRV$^+$ neurons dramatically decreased at day 7 (plus six) after SCI. In contrast to the increased PRV$^+$ neurons during the recovery period in rat SCI (Bareyre et al., 2004), however, we did not observe any increase or change in their distribution in the cerebral cortex even at days 28–42 (Fig. 4B–D). These results suggest that spontaneous CST rewiring is limited in our mouse thoracic SCI model, possibly
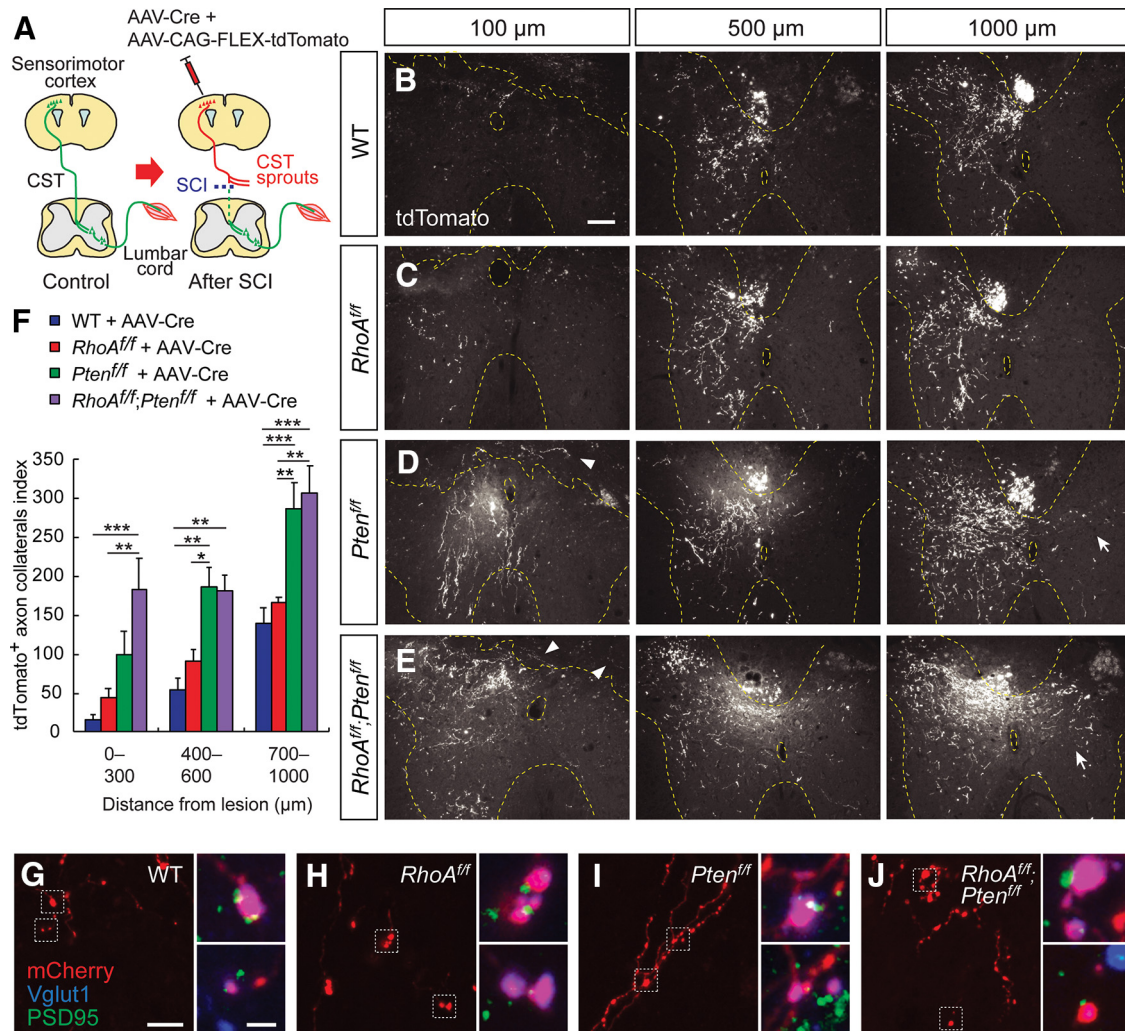
**Figure 5.** *RhoA* and *Pten* deletion additively increases rewiring of sensorimotor cortex to spinal cord to hindlimb muscle connections. ***A***–***D***, Representative images of PRV-RFP$^+$ layer V neurons with EGFP-Cre$^+$ in the sensorimotor cortex of WT (***A***), *RhoA$^{f/f}$* (***B***), *Pten$^{f/f}$* (***C***), and *RhoA$^{f/f}$;Pten$^{f/f}$* (***D***) mice injected with AAV-Cre (arrowheads). PRV was injected into the hindlimb muscle for trans-synaptic tracing. Scale bar, 50 μm. ***E***, Location of PRV$^+$/EGFP-Cre$^+$ layer V neurons in the cerebral cortex of WT, *RhoA$^{f/f}$*, *Pten$^{f/f}$*, and *RhoA$^{f/f}$;Pten$^{f/f}$* mice injected with AAV-Cre. Data from three individual animals are plotted in three different colors in the top view of the cortex. Neuronal positions were calculated by their distance from the bregma along the AP and ML axes. ***F***, Quantification of the number of PRV-RFP$^+$ EGFP-Cre$^+$ layer V neurons in the sensorimotor cortex of WT, *RhoA$^{f/f}$*, *RhoA$^{f/f}$;RhoC$^{-/-}$*, *Pten$^{f/f}$*, *RhoA$^{f/f}$;Pten$^{f/f}$* and *RhoA$^{f/f}$;Pten$^{f/f}$;RhoC$^{-/-}$* mice injected with AAV-Cre, and PRV-RFP$^+$ layer V neurons in *RhoC$^{-/-}$* mice for comparison. One-way ANOVA followed by Tukey's test, *$p < 0.05$, **$p < 0.01$; $n = 4$.

because of species-specific differences or other experimental conditions from the previous study (Bareyre et al., 2004).

Next, PRV614 was injected into the Rf muscle of AAV-Cre-injected WT, *RhoA$^{f/f}$*, *RhoA$^{f/f}$;RhoC$^{-/-}$*, *Pten$^{f/f}$*, *RhoA$^{f/f}$;Pten$^{f/f}$*, and *RhoA$^{f/f}$;RhoC$^{-/-}$;Pten$^{f/f}$* mice at day 42 postinjury. After 6 d, PRV-RFP$^+$ and EGFP-Cre$^+$ neurons were detected in layer V of the hindlimb area (Fig. 5A–D). *RhoA$^{f/f}$* and *Pten$^{f/f}$* mice did not show significant changes in numbers of PRV-RFP and EGFP-Cre double-positive neurons compared with WT controls, although *Pten$^{f/f}$* mice showed trends toward increased labeling (Fig. 5A–C, E,F; $n = 4$; $p = 0.924$ and $p = 0.294$, respectively). Interestingly, *RhoA* and *Pten* double-mutant mice had significantly increased numbers of PRV-RFP$^+$ EGFP-Cre$^+$ neurons compared with WT and *RhoA$^{f/f}$* mice (Fig. 5A–F; $n = 4$; $p = 0.0015$ and $p = 0.0182$, respectively). *RhoA$^{f/f}$;RhoC$^{-/-}$* and *RhoA$^{f/f}$;RhoC$^{-/-}$;Pten$^{f/f}$* mice did not show increased PRV$^+$ numbers ($n = 4$–5; Fig. 5F). *RhoC$^{-/-}$* SCI mice were further injected with PRV614 as a comparison, and the PRV-RFP$^+$ cell numbers did not significantly change (Fig. 5F; $p = 0.762$). These data suggest that *RhoA* and *Pten* deletions additively increase the connections within the cerebral cortex to spinal cord to hindlimb muscles circuit, whereas double knockout of *RhoA* and *RhoC* does not increase this connection.

Because the CS reorganization was promoted in *RhoA$^{f/f}$;Pten$^{f/f}$* mice, we examined the amount of CST sprouting in the rostral area of the lesion. As fluorescent reporters enable more efficient labeling of CST collaterals than BDA tracing, AAV-Cre and Cre-dependent AAV-CAG-FLEX-tdTomato were simultaneously injected into the hindlimb sensorimotor cortex of WT, *RhoA$^{f/f}$*, *Pten$^{f/f}$*, and *RhoA$^{f/f}$;Pten$^{f/f}$* mice 2 weeks before the injury (Fig. 6A), and tdTomato-labeled fibers were examined at day 56 postinjury. Cortical *Pten*, but not *RhoA* deletion, resulted in significantly increased numbers of sprouting axons ($n = 4$; Fig. 6B–D,F), with many fibers sprouting across the midline into the contralateral gray matter as reported previously (Liu et al., 2010; Fig. 6D, arrows). In addition, several regenerating CST axons were observed within the fibrotic scar (Fig. 6D, arrowheads) as observed with BDA tracing (Fig. 3J). Simultaneous deletion of *RhoA* and *Pten* further enhanced sprouting, which was especially significant in the area close to

**Figure 6.** *RhoA* and *Pten* deletion additively promotes sprouting of CST fibers after SCI in the area rostral to the lesion site. ***A***, Schematic illustration to detect CST sprouting by injection of AAV-Cre and AAV-CAG-FLEX-tdTomato. ***B–E***, Representative images of tdTomato[+] CS collateral fibers at the 100 μm (left), 500 μm (center), and 1000 μm (right) areas rostral to the lesion in WT (***B***), *RhoA*[f/f] (***C***), *Pten*[f/f] (***D***), and *RhoA*[f/f];*Pten*[f/f] (***E***) mice. Arrowheads indicate the CST fibers growing into the fibrotic scar, and arrows indicate the CST fibers elongating to the contralateral side. Scale bar, 200 μm. ***F***, Quantification of the amount of CST fibers in the gray matter at the indicated rostral area of the lesion in WT, *RhoA*[f/f], *Pten*[f/f], and *RhoA*[f/f];*Pten*[f/f] mice. One-way ANOVA followed by Tukey's test, *$p < 0.05$, **$p < 0.01$, *** $p < 0.001$; $n = 4$. ***G–J***, Vglut1^{+} presynaptic terminals of mCherry[+] CST fibers contacted with postsynaptic PSD-95^{+} puncta in the thoracic cord rostral to the injury in WT (***G***), *RhoA*[f/f] (***H***), *Pten*[f/f] (***I***), and *RhoA*[f/f];*Pten*[f/f] (***J***) mice; mCherry, red; Vglut1, blue; PSD-95, green. Right, Higher magnification images of the dotted squares on the left. Scale bar, 10 μm (left), 2 μm (right).

the lesion site (0–300 μm rostral; $n = 4$; Fig. 6*E,F*). We did not observe any fibers caudal to the lesion, although some degenerating CST axons with weak tdTomato signals remained in the dorsoventral funiculus at 300 μm∼ caudal to the lesion. These axons were not connected with axons in the rostral area in serial sections (data not shown).

The sprouting fibers of either genotype contain a number of boutons positive for the glutamatergic presynaptic marker Vglut1 (Fig. 6*G–J*; Ueno et al., 2012; Zukor et al., 2013; Du et al., 2015). The presynaptic boutons were often located in close contact with postsynaptic components marked by PSD-95 (Fig. 6*G–J*). This suggests that the sprouting fibers make synapses in the gray matter rostral to the lesion.

**Genetic deletions of *RhoA*, *RhoC* and *Pten* in the CST do not promote hindlimb motor recovery**
Finally, we examined whether *RhoA*, *RhoC*, and *Pten* deletion promote recovery of hindlimb motor functions after SCI. The BMS open-field score and a grid walking test were used to evaluate the hindlimb function and coordination. *RhoA*[f/f], *RhoA*[f/f];

*RhoC*^{−/−}, *Pten*[f/f], *RhoA*[f/f];*Pten*[f/f] and *RhoA*[f/f];*RhoC*^{−/−};*Pten*[f/f] mice with AAV-Cre injections did not enhance recovery compared with WT mice ($n = 12$–14; Fig. 7). These results indicate that the observed increased regeneration, suppressed axon dieback, or increased rewiring of CST circuit is not sufficient to enhance motor recovery after SCI.

## Discussion
Previous studies have shown that modulation of intrinsic signaling pathways can augment axon regeneration after SCI, whereas the effect of global suppression of extrinsic signaling pathways by interrupting a conserved pathway remains unclear. Although combinatorial approaches to modulate both intrinsic and multiple extrinsic pathways have been predicted to improve outcomes compared with modulation of a single pathway, this prediction has yet to be tested. Moreover, most of these prior studies have not clearly discriminated the inhibitory functions on different axon dynamics observed after injury, such as regeneration (regrowth), retraction (dieback), and sprouting (Tuszynski and
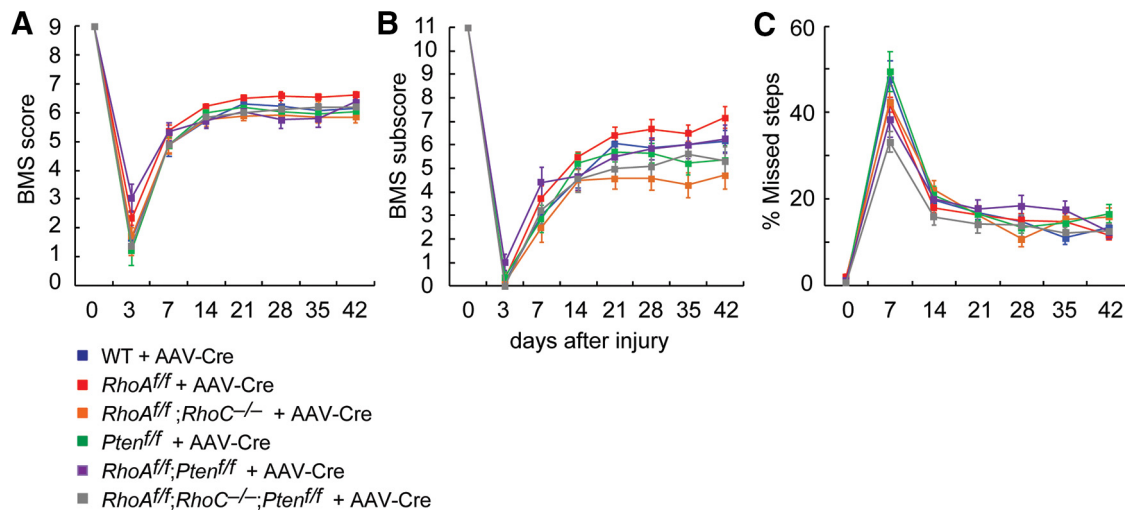
**Figure 7.** *Rho* and *Pten* deletion do not enhance recovery of hindlimb motor functions. *A*, BMS scores. *B*, BMS subscores. *C*, Grid walk test. WT, *n* = 12; *RhoA^{f/f}*, *n* = 12; *RhoA^{f/f};RhoC^{−/−}*, *n* = 14; *Pten^{f/f}*, *n* = 14; *RhoA^{f/f};Pten^{f/f}*, *n* = 12; *RhoA^{f/f};RhoC^{−/−};Pten^{f/f}*, *n* = 13; all mice were injected with AAV-Cre; two-way repeated-measures ANOVA.

Steward, 2012; Geoffroy and Zheng, 2014). Targeting specific modes of axon behavior is important in circuit reconstruction. In the present study, we comprehensively investigated whether global suppression of an extrinsic pathway, together with modulation of the main intrinsic inhibitory factor, Pten, would enable axon regrowth and adaptive rewiring of CS neurons after SCI. Our results revealed that elimination of key molecules in extrinsic and intrinsic signaling pathways affect distinct axon behaviors. *Rho* suppression reduces axon dieback, whereas *Pten* deletion induces axon regeneration. Moreover, deletion of both *RhoA* and *Pten* additively promotes rewiring of CST fibers after SCI.

*RhoA* and *RhoC* double-mutant mice retain CST axons close to the lesion, suggesting that the *RhoA* and *RhoC* double deletion suppresses axon retraction or dieback. Our previous study using *semaphorin* mutant mice and other studies suppressing Wnt signals have shown reduced axon retraction, supporting the idea that extrinsic signals drive axon retraction through Rho signals (Liu et al., 2008; Ueno et al., 2020). As injured axons show dynamic changes with retraction and regrowth (Kerschensteiner et al., 2005), we could not exclude the possibility that in addition to reduced axon retraction, *Rho* deletion may promote regeneration of some CST axons within the glial scar. However, we did not observe any CST fibers extending through the glial scar into the fibrotic lesion core or the caudal lesion boundary. These findings indicate that blockade of extrinsic signals alone does not induce regeneration across the lesion. The absence of axon regeneration in a triple myelin-associated gene deletion supports this idea (Lee et al., 2010b).

In contrast, *Pten* deletion significantly enhanced the growth ability of axons. CST fibers crossed the border of the glial and fibrotic scar, which is consistent with previous studies (Liu et al., 2010; Zukor et al., 2013). Although we did not observe any CST fibers caudal to the lesion that were previously demonstrated, we performed deletion in adult mice and not neonatal animals when mTOR signaling is greater (Liu et al., 2010). Furthermore, we observed a fibrotic scar in our dorsal hemisection model using a surgical blade, which was not apparent in some previous studies (Zukor et al., 2013; Du et al., 2015). The fibrotic scar is a robust barrier to regeneration (Dias et al., 2018), and a large lesion with fibroblasts and macrophages that lacks bridge-forming astrocytes halts regrowth of *Pten*-deleted axons (Zukor et al., 2013). These

differences may explain the lack of regenerating fibers beyond the lesion. In addition, targeting both extrinsic and intrinsic inhibitors by deleting *Rho* and *Pten* did not enable axon regeneration across the lesion core. These findings were consistent with a previous report showing that combined CSPG degradation and KLF7 overexpression does not induce axon regeneration distal to the lesion (Wang et al., 2017). Hence, a combination with additional methods is likely required to induce extensive regeneration. In this context, recent reports have succeeded to induce robust regeneration using neural progenitor cell transplantation, which provides a growth substrate bridging the lesion to sustain intrinsic growth signals (Kadoya et al., 2016; Poplawski et al., 2020), and injection of chemoattractant factors that orient growing axons to the caudal direction (Anderson et al., 2018).

In contrast to the absence of additive effects of *RhoA* and *Pten* deletion on regeneration, sprouting of CST fibers and rewiring were additively enhanced in *RhoA* and *Pten* double knockouts. This combinatorial approach is thus a promising strategy to enhance circuit plasticity within the injured spinal cord. Several studies have reported that Pten is located downstream of the Rho-ROCK pathway in the chemotaxis and migration of macrophages, leukocytes, and embryonic kidney cells (Li et al., 2005; Papakonstanti et al., 2007). It remains unknown whether this signaling cascade is also engaged in injured neurons. In our study, *Pten* deletion demonstrated stronger effects on axon growth compared with *RhoA* and *RhoA/C* knockouts. These data suggest that Pten is involved in the signaling instead the downstream of Rho.

Unfortunately, *Rho* and *Pten* deletion did not enhance hindlimb motor recovery in our thoracic SCI model, suggesting that the anatomic rewiring observed in *RhoA* and *Pten* double-mutant mice is insufficient to promote motor recovery. Many reasons may account for these results. First, the amount of rewiring and regeneration in *RhoA* and *Pten* double-mutant mice may not be sufficient for supporting the tested motor functions after SCI. Thus, in addition to *RhoA/Pten* deletion, other strategies (e. g., neural stem cell grafts, cortical or spinal stimulation) may need to be combined for motor recovery. Second, other circuits in addition to CS circuits may need to be cooperatively restored, such as rubrospinal, raphespinal, and ascending sensory fibers, as the recovery of movement depends on multiple motor and sensory pathways. Third, other *Rho* and *Pten* functions may

need to be considered. For example, *Pten* knockout triggers abnormal dendrite and cell body growth (Gallent and Steward, 2018). Rho induces dendrite simplification and spine retraction (Nakayama et al., 2000; Mulherkar et al., 2017). These attributes may also affect neuronal functions in our model. In this context, it remains unclear why *RhoA* and *RhoC* double knockout mice (i.e., *RhoA^{f/f};RhoC^{−/−}* and *RhoA^{f/f};RhoC^{−/−};Pten^{f/f}*) did not increase PRV tracing compared with WT mice. Although a single deletion of *RhoC* did not affect axon regeneration of the CST (data not shown), possibly because *RhoC* is not expressed by CST neurons, double deletion of *RhoA* and *RhoC,* which might compensatorily function by *RhoA* knockout, might suppress PRV labeling by inducing deficits in synapse formation, vesicle recycling, or retrograde transport (Tolias et al., 2011).

Redirecting axons to targets is only a piece of the puzzle. Sprouting fibers need to make proper functional connections with spinal neurons to promote motor recovery, making it important to understand how and what functional connections should be restored following injury. We previously published a detailed map of connections and functions of cervical CS circuits (Ueno et al., 2018), and another group has demonstrated that CS circuits from the sensorimotor cortex control locomotion (Karadimas et al., 2020). Although the mechanisms to create these specific connections remain unknown, reconstructing such pathways will be important for regenerative therapies in the future. Moreover, various studies have shown that rehabilitation (and related neural activities) promotes functional recovery by facilitating the establishment of functional connections (García-Alías et al., 2009; van den Brand et al., 2012). Combining targeted molecular therapeutics with rehabilitative training will be worthwhile to test in future studies. Thus far, however, growth-promoting treatments, such as targeting Pten, Sox11, or Nogo that have been combined with training, have often induced aberrant axonal growth and have either failed to enhance recovery or even worsened recovery in some cases (Wahl et al., 2014; Geoffroy et al., 2015; Jayaprakash et al., 2016). It has been proposed that growth promotion followed by a subsequent training paradigm can leverage newly formed circuits to support functional recovery (Wahl et al., 2014). Thus, temporal and spatial control of molecular manipulation is required in future studies.

With regard to clinical testing, inhibitors enable time-dependent treatments. For example, Pten inhibitors enhance axon regrowth in mouse SCI (Ohtake et al., 2014). Rho inhibitors also exhibit beneficial effects in rodent SCI models (Dergham et al., 2002; Fu et al., 2007; Boato et al., 2010). Clinical studies using VX-210 (Cethrin or BA-210), a cell-permeable derivative of the bacterial enzyme C3 transferase (Fehlings et al., 2018), remain to show an improved outcome. In this regard, controls for spatial or cell-type-specific targeting may be difficult. Rho and Pten are signaling molecules widely used in cells, uninjured neurons, glia, and inflammatory cells involved in tissue repair, which will also be influenced by the treatment (Hara et al., 2000; Fournier et al., 2003; Otsuka et al., 2011; Renault-Mihara et al., 2017). Conditional gene targeting studies on other cell types, in addition to the specific neurons tested in this study, will be required to understand the full mechanistic effects of inhibitors.

In conclusion, our study reveals the effects of extrinsic and intrinsic signals in injured axon dynamics and shows that targeting both factors is effective to promote sprouting and rewiring after SCI. Further combinatorial and regulated methods should be tested for therapeutic approaches to restore neural circuitry and functions after SCI.

## References

Anderson MA, O'Shea TM, Burda JE, Ao Y, Barlatey SL, Bernstein AM, Kim JH, James ND, Rogers A, Kato B, Wollenberg AL, Kawaguchi R, Coppola G, Wang C, Deming TJ, He Z, Courtine G, Sofroniew MV (2018) Required growth facilitators propel axon regeneration across complete spinal cord injury. Nature 561:396–400.

Atwal JK, Pinkston-Gosse J, Syken J, Stawicki S, Wu Y, Shatz C, Tessier-Lavigne M (2008) PirB is a functional receptor for myelin inhibitors of axonal regeneration. Science 322:967–970.

Bareyre FM, Kerschensteiner M, Raineteau O, Mettenleiter TC, Weinmann O, Schwab ME (2004) The injured spinal cord spontaneously forms a new intraspinal circuit in adult rats. Nat Neurosci 7:269–277.

Basso DM, Fisher LC, Anderson AJ, Jakeman LB, McTigue DM, Popovich PG (2006) Basso Mouse Scale for locomotion detects differences in recovery after spinal cord injury in five common mouse strains. J Neurotrauma 23:635–659.

Blackmore MG, Wang Z, Lerch JK, Motti D, Zhang YP, Shields CB, Lee JK, Goldberg JL, Lemmon VP, Bixby JL (2012) Krüppel-like Factor 7 engineered for transcriptional activation promotes axon regeneration in the adult corticospinal tract. Proc Natl Acad Sci U S A 109:7517–7522.

Boato F, Hendrix S, Huelsenbeck SC, Hofmann F, Grosse G, Djalali S, Klimaschewski L, Auer M, Just I, Ahnert-Hilger G, Höltje M (2010) C3 peptide enhances recovery from spinal cord injury by improved regenerative growth of descending fiber tracts. J Cell Sci 123:1652–1662.

Borisoff JF, Chan CC, Hiebert GW, Oschipok L, Robertson GS, Zamboni R, Steeves JD, Tetzlaff W (2003) Suppression of Rho-kinase activity promotes axonal growth on inhibitory CNS substrates. Mol Cell Neurosci 22:405–416.

Bradbury EJ, Moon LD, Popat RJ, King VR, Bennett GS, Patel PN, Fawcett JW, McMahon SB (2002) Chondroitinase ABC promotes functional recovery after spinal cord injury. Nature 416:636–640.

Cafferty WB, Duffy P, Huebner E, Strittmatter SM (2010) MAG and OMgp synergize with Nogo-A to restrict axonal growth and neurological recovery after spinal cord trauma. J Neurosci 30:6825–6837.

Chan CC, Khodarahmi K, Liu J, Sutherland D, Oschipok LW, Steeves JD, Tetzlaff W (2005) Dose-dependent beneficial and detrimental effects of ROCK inhibitor Y27632 on axonal sprouting and functional recovery after rat spinal cord injury. Exp Neurol 196:352–364.

Chauhan BK, Lou M, Zheng Y, Lang RA (2011) Balanced Rac1 and RhoA activities regulate cell shape and drive invagination morphogenesis in epithelia. Proc Natl Acad Sci U S A 108:18289–18294.

Dergham P, Ellezam B, Essagian C, Avedissian H, Lubell WD, McKerracher L (2002) Rho signaling pathway targeted to promote spinal cord repair. J Neurosci 22:6570–6577.

Dias DO, Kim H, Holl D, Werne Solnestam B, Lundeberg J, Carlén M, Göritz C, Frisén J (2018) Reducing pericyte-derived scarring promotes recovery after spinal cord injury. Cell 173:153–165.

Du K, Zheng S, Zhang Q, Li S, Gao X, Wang J, Jiang L, Liu K (2015) Pten deletion promotes regrowth of corticospinal tract axons 1 year after spinal cord injury. J Neurosci 35:9754–9763.

Duffy P, Schmandke A, Schmandke A, Sigworth J, Narumiya S, Cafferty WBJ, Strittmatter SM (2009) Rho-associated kinase II (ROCKII) limits axonal growth after trauma within the adult mouse spinal cord. J Neurosci 29:15266–15276.

Duffy P, Wang X, Siegel CS, Seigel CS, Tu N, Henkemeyer M, Cafferty WBJ, Strittmatter SM (2012) Myelin-derived ephrinB3 restricts axonal regeneration and recovery after adult CNS injury. Proc Natl Acad Sci U S A 109:5063–5068.

Fehlings MG, Kim KD, Aarabi B, Rizzo M, Bond LM, McKerracher L, Vaccaro AR, Okonkwo DO (2018) Rho inhibitor VX-210 in acute traumatic subaxial cervical spinal cord injury: design of the spinal cord injury Rho inhibition investigation (SPRING) clinical trial. J Neurotrauma 35:1049–1056.

Fink KL, Strittmatter SM, Cafferty WB (2015) Comprehensive corticospinal labeling with mu-crystallin transgene reveals axon regeneration after spinal cord trauma in ngr1 -/- mice. J Neurosci 35:15403–15418.

Fournier AE, Takizawa BT, Strittmatter SM (2003) Rho kinase inhibition enhances axonal regeneration in the injured CNS. J Neurosci 23:1416–1423.

Fu Q, Hue J, Li S (2007) Nonsteroidal anti-inflammatory drugs promote axon regeneration via RhoA inhibition. J Neurosci 27:4154–4164.

Fujita Y, Yamashita T (2014) Axon growth inhibition by RhoA/ROCK in the central nervous system. Front Neurosci 8:338.

Gallent EA, Steward O (2018) Neuronal PTEN deletion in adult cortical neurons triggers progressive growth of cell bodies, dendrites, and axons. Exp Neurol 303:12–28.

García-Alías G, Barkhuysen S, Buckle M, Fawcett JW (2009) Chondroitinase ABC treatment opens a window of opportunity for task-specific rehabilitation. Nat Neurosci 12:1145–1151.

Geoffroy CG, Zheng B (2014) Myelin-associated inhibitors in axonal growth after CNS injury. Curr Opin Neurobiol 27:31–38.

Geoffroy CG, Lorenzana AO, Kwan JP, Lin K, Ghassemi O, Ma A, Xu N, Creger D, Liu K, He Z, Zheng B (2015) Effects of PTEN and Nogo codeletion on corticospinal axon sprouting and regeneration in mice. J Neurosci 35:6413–6428.

Gu Z, Serradj N, Ueno M, Liang M, Li J, Baccei ML, Martin JH, Yoshida Y (2017) Skilled movements require non-apoptotic Bax/Bak pathway-mediated corticospinal circuit reorganization. Neuron 94:626–641.e4.

Hakem A, Sanchez-Sweatman O, You-Ten A, Duncan G, Wakeham A, Khokha R, Mak TW (2005) RhoC is dispensable for embryogenesis and tumor initiation but essential for metastasis. Genes Dev 19:1974–1979.

Hara M, Takayasu M, Watanabe K, Noda A, Takagi T, Suzuki Y, Yoshida J (2000) Protein kinase inhibition by fasudil hydrochloride promotes neurological recovery after spinal cord injury in rats. J Neurosurg 93:94–101.

Harel NY, Strittmatter SM (2006) Can regenerating axons recapitulate developmental guidance during recovery from spinal cord injury? Nat Rev Neurosci 7:603–616.

Hata K, Fujitani M, Yasuda Y, Doya H, Saito T, Yamagishi S, Mueller BK, Yamashita T (2006) RGMa inhibition promotes axonal growth and recovery after spinal cord injury. J Cell Biol 173:47–58.

He Z, Jin Y (2016) Intrinsic control of axon regeneration. Neuron 90:437–451.

Herrmann JE, Shah RR, Chan AF, Zheng B (2010) EphA4 deficient mice maintain astroglial-fibrotic scar formation after spinal cord injury. Exp Neurol 223:582–598.

Jayaprakash N, Wang Z, Hoeynck B, Krueger N, Kramer A, Balle E, Wheeler DS, Wheeler RA, Blackmore MG (2016) Optogenetic interrogation of functional synapse formation by corticospinal tract axons in the injured spinal cord. J Neurosci 36:5877–5890.

Kadoya K, Lu P, Nguyen K, Lee-Kubli C, Kumamaru H, Yao L, Knackert J, Poplawski G, Dulin JN, Strobl H, Takashima Y, Biane J, Conner J, Zhang SC, Tuszynski MH (2016) Spinal cord reconstitution with homologous neural grafts enables robust corticospinal regeneration. Nat Med 22:479–487.

Karadimas SK, Satkunendrarajah K, Laliberte AM, Ringuette D, Weisspapir I, Li L, Gosgnach S, Fehlings MG (2020) Sensory cortical control of movement. Nat Neurosci 23:75–84.

Katayama K, Melendez J, Baumann JM, Leslie JR, Chauhan BK, Nemkul N, Lang RA, Kuan CY, Zheng Y, Yoshida Y (2011) Loss of RhoA in neural progenitor cells causes the disruption of adherens junctions and hyperproliferation. Proc Natl Acad Sci U S A 108:7607–7612.

Kerschensteiner M, Schwab ME, Lichtman JW, Misgeld T (2005) In vivo imaging of axonal degeneration and regeneration in the injured spinal cord. Nat Med 11:572–577.

Lee JK, Chow R, Xie F, Chow SY, Tolentino KE, Zheng B (2010a) Combined genetic attenuation of myelin and semaphorin-mediated growth inhibition is insufficient to promote serotonergic axon regeneration. J Neurosci 30:10899–10904.

Lee JK, Geoffroy CG, Chan AF, Tolentino KE, Crawford MJ, Leal MA, Kang B, Zheng B (2010b) Assessing spinal axon regeneration and sprouting in Nogo-, MAG-, and OMgp-deficient mice. Neuron 66:663–670.

Lesche R, Groszer M, Gao J, Wang Y, Messing A, Sun H, Liu X, Wu H (2002) Cre/loxP-mediated inactivation of the murine Pten tumor suppressor gene. Genesis 32:148–149.

Leslie JR, Imai F, Zhou X, Lang RA, Zheng Y, Yoshida Y (2012) RhoA is dispensable for axon guidance of sensory neurons in the mouse dorsal root ganglia. Front Mol Neurosci 5:67.

Li Z, Dong X, Dong X, Wang Z, Liu W, Deng N, Ding Y, Tang L, Hla T, Zeng R, Li L, Wu D (2005) Regulation of PTEN by Rho small GTPases. Nat Cell Biol 7:399–404.

Liu K, Lu Y, Lee JK, Samara R, Willenberg R, Sears-Kraxberger I, Tedeschi A, Park KK, Jin D, Cai B, Xu B, Connolly L, Steward O, Zheng B, He Z (2010) PTEN deletion enhances the regenerative ability of adult corticospinal neurons. Nat Neurosci 13:1075–1081.

Liu Y, Wang X, Lu CC, Kerman R, Steward O, Xu XM, Zou Y (2008) Repulsive Wnt signaling inhibits axon regeneration after CNS injury. J Neurosci 28:8376–8382.

McKerracher L, Ferraro GB, Fournier AE (2012) Rho signaling and axon regeneration. Int Rev Neurobiol 105:117–140.

Melendez J, Stengel K, Zhou X, Chauhan BK, Debidda M, Andreassen P, Lang RA, Zheng Y (2011) RhoA GTPase is dispensable for actomyosin regulation but is essential for mitosis in primary mouse embryonic fibroblasts. J Biol Chem 286:15132–15137.

Monnier PP, Sierra A, Schwab JM, Henke-Fahle S, Mueller BK (2003) The Rho/ROCK pathway mediates neurite growth-inhibitory activity associated with the chondroitin sulfate proteoglycans of the CNS glial scar. Mol Cell Neurosci 22:319–330.

Mulherkar S, Liu F, Chen Q, Narayanan A, Couvillon AD, Shine HD, Tolias KF (2013) The small GTPase RhoA is required for proper locomotor circuit assembly. PLoS One 8:e67015.

Mulherkar S, Firozi K, Huang W, Uddin MD, Grill RJ, Costa-Mattioli M, Robertson C, Tolias KF (2017) RhoA-ROCK inhibition reverses synaptic remodeling and motor and cognitive deficits caused by traumatic brain injury. Sci Rep 7:10689.

Nakamura T, Colbert MC, Robbins J (2006) Neural crest cells retain multipotential characteristics in the developing valves and label the cardiac conduction system. Circ Res 98:1547–1554.

Nakamura Y, Fujita Y, Ueno M, Takai T, Yamashita T (2011) Paired immunoglobulin-like receptor B knockout does not enhance axonal regeneration or locomotor recovery after spinal cord injury. J Biol Chem 286:1876–1883.

Nakayama AY, Harms MB, Luo L (2000) Small GTPases Rac and Rho in the maintenance of dendritic spines and branches in hippocampal pyramidal neurons. J Neurosci 20:5329–5338.

Ohtake Y, Park D, Abdul-Muneer PM, Li H, Xu B, Sharma K, Smith GM, Selzer ME, Li S (2014) The effect of systemic PTEN antagonist peptides on axon growth and functional recovery after spinal cord injury. Biomaterials 35:4610–4626.

Otsuka S, Adamson C, Sankar V, Gibbs KM, Kane-Goldsmith N, Ayer J, Babiarz J, Kalinski H, Ashush H, Alpert E, Lahav R, Feinstein E, Grumet M (2011) Delayed intrathecal delivery of RhoA siRNA to the contused spinal cord inhibits allodynia, preserves white matter, and increases serotonergic fiber growth. J Neurotrauma 28:1063–1076.

Oudega M, Perez MA (2012) Corticospinal reorganization after spinal cord injury. J Physiol 590:3647–3663.

Papakonstanti EA, Ridley AJ, Vanhaesebroeck B (2007) The p110delta isoform of PI 3-kinase negatively controls RhoA and PTEN. EMBO J 26:3050–3061.

Park KK, Liu K, Hu Y, Smith PD, Wang C, Cai B, Xu B, Connolly L, Kramvis I, Sahin M, He Z (2008) Promoting axon regeneration in the adult CNS by modulation of the PTEN/mTOR pathway. Science 322:963–966.

Paxinos G, Franklin KBJ (2001) The mouse brain in stereotaxic coordinates. Academic. 2nd edition. Academic Press. San Diego.

Poplawski GHD, Kawaguchi R, Van Niekerk E, Lu P, Mehta N, Canete P, Lie R, Dragatsis I, Meves JM, Zheng B, Coppola G, Tuszynski MH (2020) Injured adult neurons regress to an embryonic transcriptional growth state. Nature 581:77–82.

Porter R, Lemon R (1993) Corticospinal function and voluntary movement. Oxford, England: Oxford UP.

Renault-Mihara F, Mukaino M, Shinozaki M, Kumamaru H, Kawase S, Baudoux M, Ishibashi T, Kawabata S, Nishiyama Y, Sugai K, Yasutake K, Okada S, Nakamura M, Okano H (2017) Regulation of RhoA by STAT3 coordinates glial scar formation. J Cell Biol 216:2533–2550.

Silver J, Schwab ME, Popovich PG (2014) Central nervous system regenerative failure: role of oligodendrocytes, astrocytes, and microglia. Cold Spring Harb Perspect Biol 7:a020602.

Steward O, Zheng B, Tessier-Lavigne M, Hofstadter M, Sharp K, Yee KM (2008) Regenerative growth of corticospinal tract axons via the ventral column after spinal cord injury in mice. J Neurosci 28:6836–6847.

Tennant KA, Adkins DL, Donlan NA, Asay AL, Thomas N, Kleim JA, Jones TA (2011) The organization of the forelimb representation of the C57BL/6 mouse motor cortex as defined by intracortical microstimulation and cytoarchitecture. Cereb Cortex 21:865–876.

Tolias KF, Duman JG, Um K (2011) Control of synapse development and plasticity by Rho GTPase regulatory proteins. Prog Neurobiol 94:133–148.

Tuszynski MH, Steward O (2012) Concepts and methods for the study of axonal regeneration in the CNS. Neuron 74:777–791.

Ueno M, Hayano Y, Nakagawa H, Yamashita T (2012) Intraspinal rewiring of the corticospinal tract requires target-derived brain-derived neurotrophic factor and compensates lost function after brain injury. Brain 135:1253–1267.

Ueno M, Nakamura Y, Li J, Gu Z, Niehaus J, Maezawa M, Crone SA, Goulding M, Baccei ML, Yoshida Y (2018) Corticospinal circuits from the sensory and motor cortices differentially regulate skilled movements through distinct spinal interneurons. Cell Rep 23:1286–1300.e7.

Ueno M, Nakamura Y, Nakagawa H, Niehaus JK, Maezawa M, Gu Z, Kumanogoh A, Takebayashi H, Lu QR, Takada M, Yoshida Y (2020) Olig2-induced semaphorin expression drives corticospinal axon retraction after spinal cord injury. Cereb Cortex 30:5702–5716.

Usher LC, Johnstone A, Ertürk A, Hu Y, Strikis D, Wanner IB, Moorman S, Lee JW, Min J, Ha HH, Duan Y, Hoffman S, Goldberg JL, Bradke F,

Chang YT, Lemmon VP, Bixby JL (2010) A chemical screen identifies novel compounds that overcome glial-mediated inhibition of neuronal regeneration. J Neurosci 30:4693–4706.

van den Brand R, Heutschi J, Barraud Q, DiGiovanna J, Bartholdi K, Huerlimann M, Friedli L, Vollenweider I, Moraud EM, Duis S, Dominici N, Micera S, Musienko P, Courtine G (2012) Restoring voluntary control of locomotion after paralyzing spinal cord injury. Science 336:1182–1185.

Wahl AS, Omlor W, Rubio JC, Chen JL, Zheng H, Schröter A, Gullo M, Weinmann O, Kobayashi K, Helmchen F, Ommer B, Schwab ME (2014) Neuronal repair. Asynchronous therapy restores motor control by rewiring of the rat corticospinal tract after stroke. Science 344:1250–1255.

Wang Z, Reynolds A, Kirry A, Nienhaus C, Blackmore MG (2015) Overexpression of Sox11 promotes corticospinal tract regeneration after spinal injury while interfering with functional recovery. J Neurosci 35:3139–3145.

Wang Z, Winsor K, Nienhaus C, Hess E, Blackmore MG (2017) Combined chondroitinase and KLF7 expression reduce net retraction of sensory and CST axons from sites of spinal injury. Neurobiol Dis 99:24–35.

Zukor K, Belin S, Wang C, Keelan N, Wang X, He Z (2013) Short hairpin RNA against PTEN enhances regenerative growth of corticospinal tract axons after spinal cord injury. J Neurosci 33:15350–15361.